RSC Advances

ROYAL SOCIETY OF CHEMISTRY

www.rsc.org/advances

Journal name

Paper

Valence variation of phase-pure M1 MoVNbTe oxide by plasma treatment for improved catalytic performance in oxidative dehydrogenation of ethane

Received 00th July 20xx,
Accepted 00th October 20xx

DOI: 10.1039/x0xx00000x

www.rsc.org/

Xin Chen, Qianli Yang, Bozhao Chu, Hang An and Yi Cheng*

This work presents a new method of catalyst surface modification by using oxygen plasma to change the oxidation state of active sites in metal oxide catalyst. The concentration of V^{5+} ions on phase-pure M1 MoVNbTeOx catalyst is the key factor of catalytic performance of oxidative dehydrogenation of ethane (ODHE) process. Based on this variable valence system, oxygen plasma is used to increase the vanadium valence state in consideration of its strong oxidization property at low temperature. As expected, the oxygen plasma can efficiently increase the V^{5+}/V^{4+} ratio on the catalyst surface without influencing the M1 phase structure. The catalyst evaluation results confirm that the oxidized catalysts give better performance in ODHE process, e.g., a 9% increase of ethane conversion using the catalyst treated by 50% O_2 plasma compared to the M1 phase catalyst without any post treatment under the conditions of 673 K and the contact time of 20.7 g_{cat}·h/mol_{C2H6}. As a gas-solid method, plasma treatment provides an efficient and mild way for catalyst preparation and modification. It is anticipated that this novel approach can be extended to treat a rich variety of redox catalysts.

1. Introduction

Ethylene is one of the largest-volume raw materials worldwide in petrochemical industry [1] . While the low selectivity and high energy consumption of traditional steam cracking method[2] have stimulated R&D activities for new methods to produce olefins, such as catalytic dehydrogenation[3], oxidative dehydrogenation[4] or CO_2 oxidative dehydrogenation[5, 6]. Focusing on the oxidative dehydrogenation process, various catalysts have been investigated, including unreducible metal oxide catalysts consisting of an alkali metal or alkaline earth metal (i.e. Li, Na, Mg)[7-9], and reducible metal oxide catalysts consisting of transition metals (i.e. Ni, Mo, V)[10-17]. MoVNbTe oxide is among the most promising catalysts for ethane or propane oxidative dehydrogenation[6] and the (amm)oxidation of propane[18], which is also extensively studied in our group[19-21]. As generally accepted, the catalyst mainly consists of two crystalline phases known as M1 and M2[22-24]. The M1 phase is an orthorhombic phase, in which corner sharing MO_6 octahedrons (M = Mo, V) assembling at (001) plane build the pentagonal rings occupied by Nb-O units as well as hexagonal rings hosting Te-O units. The M2 phase only contains hexagonal rings without pentagonal or heptagonal rings on (001) plane[22].

The V^{5+} ions in M1 phase are considered as the active sites for alkane activation, while the M2 phase contains no Nb element or V^{5+} ions, but more Te occupying the hexagonal channels, which is considered as the active sites for the activation of α-H in the alkane[25, 26]. Pure M1 phase catalyst has been acknowledged as a better choice for ethane oxidative dehydrogenation because ethane has no α-H thus M2 phase does not work in this process[13]. Nguyen et al. [27] explained the correlation between the V^{5+} surface content and the alkane conversion by varying the total surface vanadium content. Meanwhile our previous work has shown that the V^{5+} concentration is the main factor influencing the phase-pure M1 catalyst activity[20]. Therefore, increasing the V^{5+} abundance on the catalyst surface would be an effective way to improve the performance of phase-pure M1 MoVNbTeOx catalyst. Considering that the structure of the catalyst system is sensitive to the preparation procedure[28] , the means to modify the catalyst needs to be performed under mild conditions.

Non-thermal plasma is known as an ionized gas consisting of energetic components such as electrons, ions, free radicals, neutral byproducts and photons. The physical interaction via active species in the gas phase sputtering to the solid surface and the chemical interaction through radical or chemical reaction with the contamination make it capable of surface modification[29]. Over the years, non-thermal plasma and catalyst interactions have been discussed frequently and showed many interesting results[30-34]. For example, H_2 and/or Ar plasma was used to totally reduce the catalyst for methane reforming[35] and Fischer–Tropsch synthesis[34], resulting in the improvement of catalyst dispersion and increase in surface area by reducing the particle size. As a result, the catalytic reactivity and stability were enhanced. Holzer et al. [36] used manganese oxide catalyst in plasma for VOC oxidation, indicating that manganese metal center was in a higher oxidation state than in the normal dioxide during the reaction. While Guo et al. [37] combined DBD discharge and manganese oxides for toluene decomposition, concluding that Mn_2O_3 was reduced to a lower-valent manganese oxide like Mn_3O_4. Lin et al.[38] used oxygen plasma

[a] Department of Chemical Engineering, Tsinghua University, Beijing 100084, PR China. Email: yiceng@tsinghua.edu.cn Fax: 86 10 62772051; Tel: 86 10 62794468

to increase the oxygen vacancy in order to activate the CuO-ZnO inverse opals for methanol reforming, and the result showed that the electrons were transferred from ZnO to CuO during the plasma treatment, thus increased the density of oxygen vacancy on ZnO surface. Zou et al. [39] indicated that even oxygen plasma could reduce the noble metal ions. So far, few reports have discussed about controllable plasma oxidation of catalyst, and how the plasma would influence valences of the elements in catalyst is still not explored yet.

Based on the variable valence site of the catalyst system, this work makes the first try to investigate the impact of oxygen plasma on phase-pure M1 MoVNbTeOx catalyst in the ODHE process. It is anticipated that the proposed novel methodology can be extended to a variety of catalyst applications in redox reaction processes.

2. Experimental

2.1 Catalyst preparation

Before plasma treatment, the MoVNbTeOx catalyst was prepared by hydrothermal synthesis and purified by removal of the M2 phase using H_2O_2 to form the phase-pure M1 catalyst. Aqueous slurry comprising Mo, V, Te and Nb in the molar ratios Mo:V:Te:Nb=1:0.25:0.23:0.12 was prepared, using ammonium heptamolybdate (Sigma-Aldrich, 99.0%), vanadyl sulfate (Sigma-Aldrich, 97%) telluric acid (Sigma-Aldrich, 98%) and ammonium niobium oxalate (Sigma-Aldrich, 99.99%). The precursor slurry was put into a 100-ml Teflon-lined autoclave, in which nitrogen was used to replace the residual air. Hydrothermal synthesis was carried out at 175 °C for 48 h. The obtained powder sample was filtered and washed thoroughly with distilled water, dried for 16 h at 80 °C in air, and then calcinated at 600 °C for 2 h in nitrogen atmosphere. After dissolving the M2 phase in the 5% H_2O_2 at 60 °C for 2 h, and drying the remained powder overnight at 80 °C, the phase-pure M1 catalyst was obtained [19-20].

The plasma treatment was carried out at atmospheric pressure and room temperature in a quartz reactor fixed on a vibration platform. Fig. 1 shows the diagram of the reactor. There are three grooves in the reactor. The middle one is the plasma discharge area, the size of which is 50 mm × 50 mm. Baffles of the grooves are made of quartz sand. 0.35 g phase-pure M1 catalyst was put in the middle groove of the reactor each time for plasma treatment. During plasma treatment, the power voltage, current and corresponding frequency were 35 kV, 1.9 A and 9.5 kHz, respectively. The total flow rate of carrier gas was fixed at 60 ml/min. The sample catalysts were treated by Ar plasma for 40 min, pure O_2 plasma for 40 min, 50% O_2/50% Ar plasma for 40 min and 80 min, and ozone for 80 min, named as Ar-P-40, O_2(1)-P-40, O_2(0.5)-P-40, O_2(0.5)-P-80 and O_3-80, respectively. The sample catalyst of O_3-80 was made in the following way: the ozone was generated by 50% O_2/50% Ar plasma, while the catalyst was put in the right groove, which is the downstream of the discharge area. In addition, to avoid the error caused by the instability of different batches of reagents and manual operations, all the catalysts with post treatment were from the same batch of the untreated catalyst.

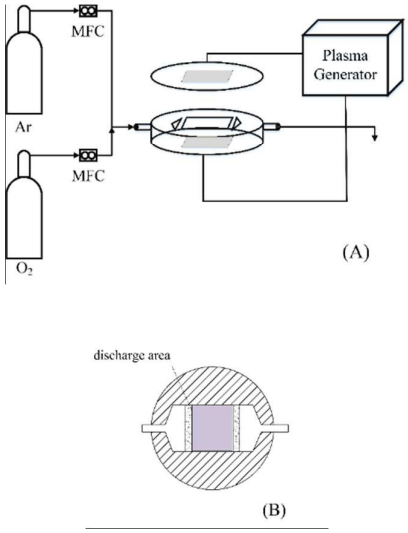

Fig. 1 Schematic diagram of plasma treatment reactor
(A) flow diagram; (B) cross section of quartz reactor

2.2 Catalyst testing

The experiments were carried out at atmospheric pressure isothermally. 0.5 g catalyst diluted with 5 g SiC powder was loaded in a quartz tube (6 mm i.d. and 750 mm length). The gas feed consisted of ethane, oxygen and helium with a C_2H_6/O_2/He molar ratio of 30/20/50. The total flow rate was varied from 30 ml/min to 90 ml/min, correspondingly the space time W/F_{C2H6} (W is the catalyst mass and F_{C2H6} is the ethane molar flow rate) was varied from 20.7 g_{cat}·h/mol_{C2H6} to 6.91 g_{cat}·h/mol_{C2H6}. The reaction temperature was maintained at 673 K. Helium was the only gas fed through the reactor tube during the heating up of the fixed-bed reactor. Once the reaction temperature was reached, the gas feed with the appropriate composition was introduced into the system. The steady-state data of catalyst performance were determined after 8 h since the beginning of the reaction, as there is usually an induction period for the catalysts in oxidative dehydrogenation of alkanes. The effluent gas from the reactor was analyzed by an online gas chromatography (GC) equipped with two columns. A PorapakQ column was used to separate the CO_2, C_2H_4 and C_2H_6 and a 5A molecular sieve column was used to separate the O_2, N_2, CH_4 and CO. For a certain catalyst, when the experiment condition was changed, we wait for 2 h to ensure that the steady state of conversion has been reached. At each condition, the constituent of effluent gas was analyzed for 3 times to affirm that the conversion was within a limit of 0.2% fluctuation.

The conversion and selectivity for ODHE process are defined as follows:

$$X_{C_2H_6} = \left(1 - \frac{2f_{C_2H_6}}{2f_{C_2H_6} + 2f_{C_2H_4} + f_{CO} + f_{CO_2}}\right) \times 100\% \quad (1)$$

$$S_{C_2H_4} = \left(\frac{2f_{C_2H_6}}{2f_{C_2H_4} + f_{CO} + f_{CO_2}}\right) \times 100\% \quad (2)$$

where *X* is the ethane conversion, *S* is the ethylene selectivity, and *f* is the molar fraction in the effluent gas.

2.3 Catalyst characterization

X-ray photoelectron spectra (XPS) measurement was performed using a PHI Quantera SXM system, equipped with Al Kα X-ray source. The peak positions reported in this work were measured with a precision of ±0.2 eV for all spectra. The binding energy (BE) scale was corrected by setting the C (1s) signal at 284.6 eV. The binding energy data of reference material was obtained from NIST X-ray Photoelectron Spectroscopy Database. Survey scans (0-1200 eV) and high-resolution Mo (3d), V (2p), Te (3d), Nb (3d) and C (1s) spectra were obtained. During the high-resolution scanning for vanadium, the dwell time was increased from 300 ms to 500 ms and the number of scan times was increased from 6 to 10. The analysis of the measured high-resolution spectra was performed using XPSPEAK 4.1 software.

X-ray diffraction (XRD) patterns of samples were recorded on a Bruker D8 Advance equipment with Cu Kα radiation. 2θ scans were run from 5–50 degrees at a rate of 0.2 degree per minute. The spectra were identified with JCPDS database (Joint Committee of Powder Diffraction Standards) and the ICSD database (Inorganic Crystal Structure Database). M1 phase (ICSD 55097) has characteristic diffraction lines located at 2θ = 6.6, 7.7, 8.9, 22.1, and 27.1° and the M2 phase (ICSD 55098) at 2θ = 22.1, 28.1and 36.2°, according to the ICSD database.

The specific surface area of the samples was calculated by Multipoint Brunauer–Emmett–Teller (BET) method in the p/p_0 = 0.05-0.30 pressure range. Nitrogen adsorption was carried out at 77 K on a Quantachrome Autosorb-6B analyzer. Prior to the measurement, the samples were degassed in vacuum at 383 K for 2 h.

Metal contents were measured by inductively coupled plasma-optical emission spectrometry (ICP-OES, Varian Vista RL spectrometer).

Scanning electron microscopy (SEM, JEOL, JSM-7401F) and JEOL JEM2010 high-resolution transmission electron microscopy (HR-TEM) were used to characterize the samples' morphology and particle size.

3. Results and Discussion

3.1 XPS analysis

As discussed above, V^{5+} abundance is the key factor relevant to the catalyst activity. To verify the oxidative effect of oxygen plasma in our system, we prepared O_2(0.5)-P-40, O_2(0.5)-P-80 and O_2(1)-P-40 catalysts to see the influences of plasma treatment time and oxygen concentration. A catalyst sample (O_3-80) was prepared by ozone treatment, where the ozone was generated by 50% oxygen plasma, in order to compare the oxidization difference. Moreover, a catalyst sample treated by Ar plasma (Ar-P-40) was made to see if the electrons generated in plasma would influence the valence state of elements.

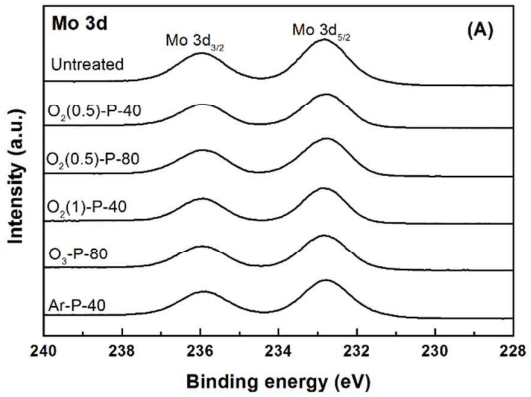

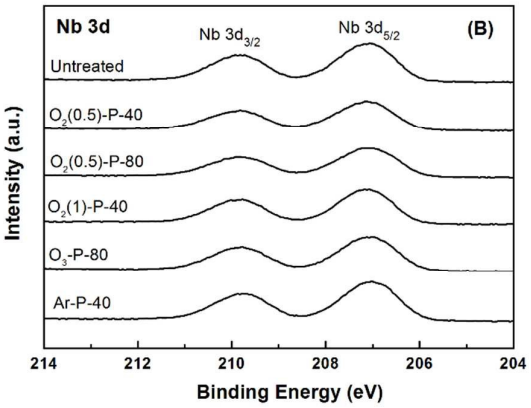

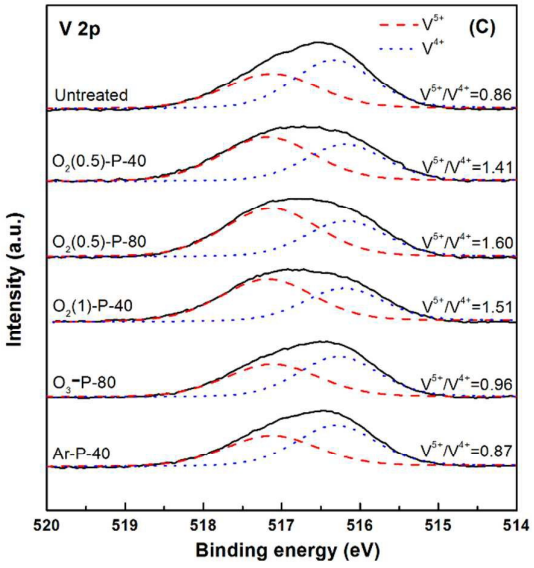

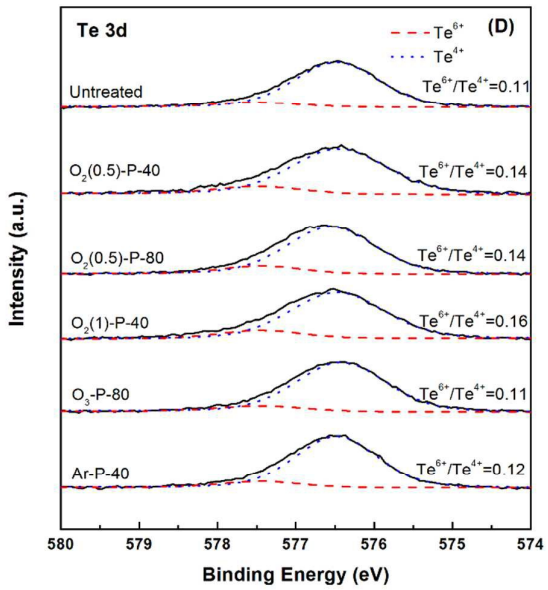

Fig. 2 XPS spectra of (A) Mo 3d (B) Nb 3d (C) V 3p (D) Te 3d

Fig. 2 shows XPS spectra of the main transition metal elements. Mo and Nb elements are indispensable elements to build the M1 structure[22, 25]. The binding energies (BEs) of molybdenum (232.8±0.1 eV) and niobium (207.1±0.1 eV) for all catalysts correspond well to the ones for MoO_3 and Nb_2O_5 reported before[40], suggesting that molybdenum and niobium exist in single valence states of +6 and +5, respectively.

Two valence states of vanadium exist in the catalyst, corresponding to the value of 516.3±0.1 eV for V^{4+} species and 517.1±0.1 eV for V^{5+} species in the spectra. The abundance of the V^{5+} species and V^{4+} species on the respective catalyst surfaces was calculated by combination of the elemental composition and de-convolution of the vanadium $2p_{3/2}$ peak. The Full Width at Half Maximum (FWHM) was fixed at 1.4±0.1 eV for V^{5+} and 1.2±0.1 eV for V^{4+}. The V^{5+}/V^{4+} ratio was calculated by the area ratio of the calculated peaks.

It can be seen from the spectra that there is an obvious increase of the V^{5+}/V^{4+} ratio in the catalysts treated by oxygen plasma. As expected, a longer plasma treatment time would lead to a higher V^{5+}/V^{4+} ratio. While if the treatment time is same, the percentage of V^{5+} content increases with the oxygen concentration. The O_3 treated catalyst results in a modest increase of V^{5+}/V^{4+} ratio, showing that O_3 gas generated by plasma could oxidize the surface vanadium as well, but is less effective compared to the oxygen plasma.

As a variable-valence metal, the valance state of vanadium can be regulated. Oxygen plasma contains many active species such as ozone, oxygen atoms O(^{3}P, ^{1}D) and metastable oxygen molecules $O_2(a^1\Delta_g, b^1\Delta_g^+)$[41], in which the oxygen atom's oxidation potential is higher than that of ozone[42]. These species are so active and oxidative that the oxygen plasma behaves far more efficient in the oxidation of MoVNbTe oxide than ozone alone.

Zhu et al. claimed that the electrons generated in the cold plasma could reduce the Pt/Al_2O_3 catalyst[43] and Zou et al. indicated that even oxygen plasma can reduce the noble metal ions[39]. To make clear if the ions in the plasma could affect the valence state of the elements on the catalyst surface, we characterized the catalyst treated by Ar plasma. The XPS spectra and V^{5+}/V^{4+} ratios show no difference between the M1 catalyst without any post-treatment and the catalyst treated by Ar plasma, suggesting that the electrons in the plasma could not reduce the vanadium on catalyst surface in our system. The effect of the V^{5+} quantity on the catalytic activity is further discussed in section 3.3.

The Tellurium exits mostly in the form of Te^{4+}, and in a small amount of Te^{6+}, with the binding energy of 576.6±0.1 eV for TeO_2 and 577.6±0.1 eV for TeO_3. The FWHM is fixed at 1.2±0.1 eV and 1.3±0.1 eV, respectively. After the plasma or ozone treatment, the valance state rarely changes, with a slight increase in Te^{6+} abundance, as shown in Fig. 2(D). Although Te element is not a paraffin activating site, it plays an important role to stabilize the phase-pure M1 catalyst, as has discussed in our previous work[21].

3.2 General properties of MoVNbTeOx catalysts

The chemical and structural details of the prepared catalysts are gathered on Table 1. The XRD patterns, TEM and SEM images of respective catalysts are presented in Fig. 3 and 4.

MoVNbTeOx catalyst is a non-stoichiometric polyoxometalate, the chemical composition of which is restricted to a certain ratio of $MoV_{0.1\text{-}0.5}Te_{0.08\text{-}0.20}Nb_{0.10\text{-}0.30}O_x$[44]. As demonstrated in our previous work[20], the 5% H_2O_2 can completely resolve the M2 phase and then produce a pure M1 phase. The catalysts prepared in this work are also within the limits of the M1 phase composition. It can be seen from Table 1 that there are no obvious changes in terms of chemical composition in the catalysts after various treatments, indicating that there is no element loss during the treatments. The XRD patterns of the catalysts treated by plasma of different carrier gases show no difference with the catalyst without any post treatment or the catalyst treated by ozone. Only the M1 phase (ICSD-55097) exists in various catalyst powders as no characteristic peak of the M2 phase (ICSD-55098) can be observed, which indicates that the plasma treatment does not induce crystal form transformation. As displayed in Fig. 4, the typical needle-shape morphology of the M1 crystals is shown in SEM images and the typical lattice planes are shown in TEM images. The average particle sizes and the surface areas analyzed by SEM and BET also show no differences, indicating that the plasma treatment does not destruct the catalyst structure.

In a word, the catalyst structure of M1 phase would not be influenced by plasma treatment, which is very important for the catalytic performance of the MoVNbTeOx catalyst.

Table 1 General properties of different treated MoVNbTeOx catalysts

	Bulk Composition (ICP)	Surface Composition (XPS)	Particle diameter (SEM)[a], nm	Particle Length (SEM)[a], nm	Surface Area (BET), m^2/g	V^{5+}/V^{4+} ratio
Untreated	$MoV_{0.21}Te_{0.22}Nb_{0.09}$	$MoV_{0.12}Te_{0.10}Nb_{0.29}$	83	221	28	0.86
O_2(0.5)-P-40	$MoV_{0.22}Te_{0.24}Nb_{0.09}$	$MoV_{0.11}Te_{0.11}Nb_{0.30}$	77	207	25.9	1.41
O_2(0.5)-P-80	$MoV_{0.21}Te_{0.22}Nb_{0.08}$	$MoV_{0.11}Te_{0.11}Nb_{0.29}$	85	209	26.6	1.60
O_2(1)-P-40	$MoV_{0.21}Te_{0.24}Nb_{0.09}$	$MoV_{0.11}Te_{0.11}Nb_{0.29}$	84	212	27.4	1.51
O_3-80	$MoV_{0.21}Te_{0.25}Nb_{0.09}$	$MoV_{0.11}Te_{0.12}Nb_{0.29}$	81	204	27.6	0.96
Ar-P-40	$MoV_{0.21}Te_{0.22}Nb_{0.09}$	$MoV_{0.11}Te_{0.11}Nb_{0.29}$	81	217	27.9	0.87

a. Determined based on the average diameter of at least 100 particles from the SEM images.

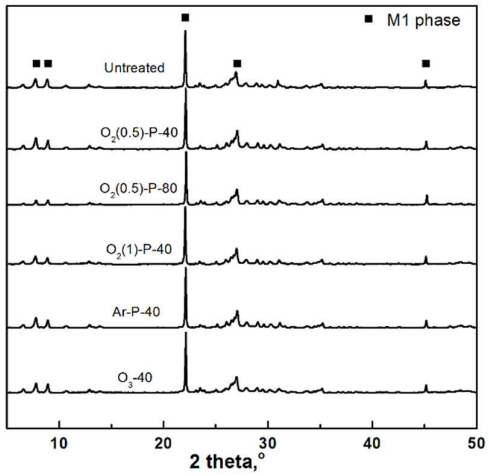

Fig. 3 XRD patterns the $MoVNbTeO_x$ catalysts

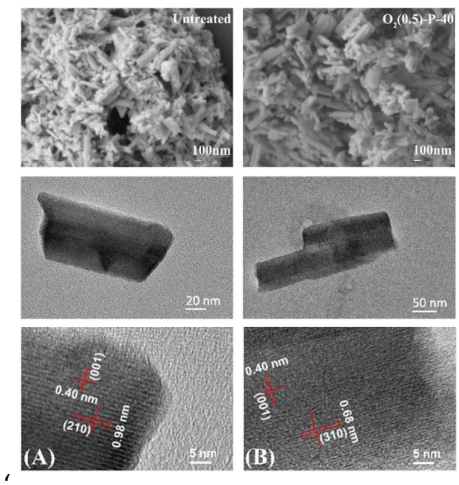

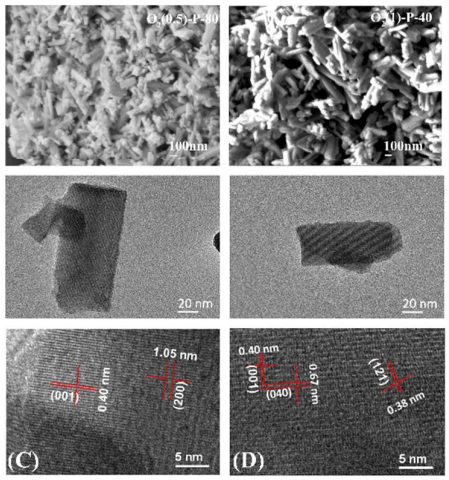

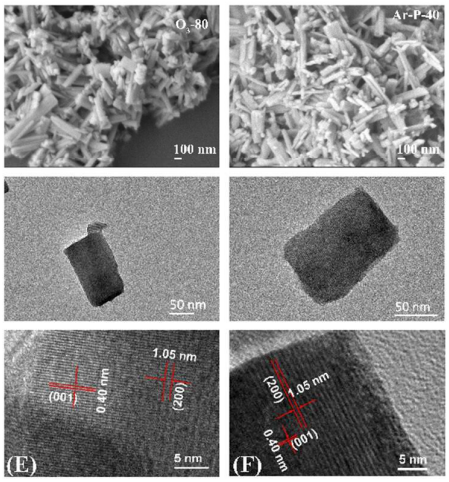

Fig. 4 TEM and SEM images of the fresh $MoVNbTeO_x$ catalysts (A) Untreated (B) O_2(0.5)-P-40 (C) O_2(0.5)-P-80 (D) O_2(1)-P-40 (E) O_3-80 (F)Ar-P-40

3.3 Catalytic evaluation of MoVNbTeOx catalysts

After affirming that the oxygen plasma could definitely oxidize the catalyst MoVNbTeOx without destroying the catalyst structure, we applied the oxidized catalysts treated by plasma and ozone to ODHE process to test the catalysts respectively. The results are presented in Fig. 5. All the oxidized catalysts show improved catalytic activity in the ODHE process compared to the untreated catalyst. The O_2(0.5)-P-80 catalyst shows an ethane conversion of 53.1%, reaching a 9-percent improvement compared with the untreated catalyst for 44.4% when the contact time is 20.7 g_{cat}·h/mol_{C2H6}. As expected, the O_2(0.5)-P-40 catalyst reaches a lower ethane conversion because of the less abundance of V^{5+}. By increasing the oxygen concentration, the O_2(1)-P-40 catalyst shows better performance than O_2(0.5)-P-40. The ozone treated catalyst also receives a 2 to 3 percent increase in terms of ethane conversion.

Fig. 6 shows the ethylene selectivity as a function of ethane conversion. The oxidized catalysts show little difference in selectivity, despite that the catalyst treated by ozone shows a slightly higher selectivity. This is probably attributed to the smoother treatment condition without high-energy plasma sputtering on the catalyst surface.

Fig. 7 shows the catalytic performance as a function of V^{5+} abundance. It can be seen that the ethane conversion is well coincident with the V^{5+}/ V^{4+} ratio.

Owing to its resonance structure (V^{5+}=O ↔ $^{4+}$V•–O•), the oxygen of V^{5+} site can easily attract a methy-H from an approaching ethane molecule, thereby abstracting it as an H·[22, 25]. According to the Mars–van Krevelen (MvK) mechanism, the reaction takes place through alternating the catalyst's active sites from oxidized to reduced states cyclically, while lattice oxygen is restored by gas phase oxygen [45] like the following equation[46]:

$C_2H_6+2OH^- \rightarrow C_2H_4+2H_2O+2e^-$ (3)

V^{4+}-(OH)+$OH^- \rightarrow V^{5+}$=(O)+e^-+H_2O (4)

V^{5+}=(O)+e^-+H2O→V^{4+}-(OH)+OH- (5)

$O_2+H_2O+4e^- \rightarrow 4OH^-$ (6)

$4V^{4+}$-(OH)+$O_2 \rightarrow 4V^{5+}$=(O)+e^-+$2H_2O$ (7)

Hence, at its highest oxidation state, V^{5+} sites strongly impart radical characteristics to its oxygen that is capable of attacking the methyl-H of a paraffin. In our experiments, after the treatment by oxygen plasma, a part of vanadium on the surface of the catalyst has been transformed from V^{4+} to V^{5+} with the catalyst structure maintained, creating more paraffin activation sites, therefore obtaining an enhanced catalytic performance of the ODHE process. Different from the physical modification by plasma treatment, the valence change induced by the oxygen plasma is persistent and the oxidative atmosphere in the experiment can maintain the change.

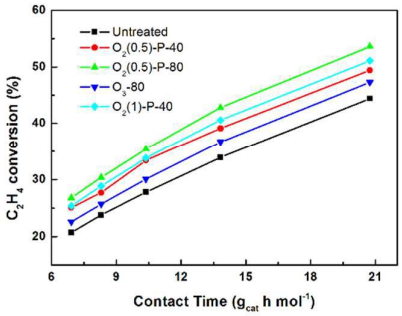

Fig. 5 $MoVNbTeO_x$ catalysts performance in the ODHE process as a function of contact time at T = 673K and feed molar ratio of $C_2H_6/O_2/He$ = 30/20/50.

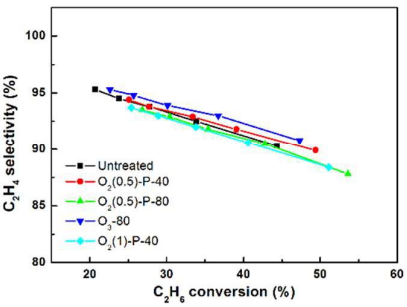

Fig. 6 Ethylene selectivity as a function of ethane conversion

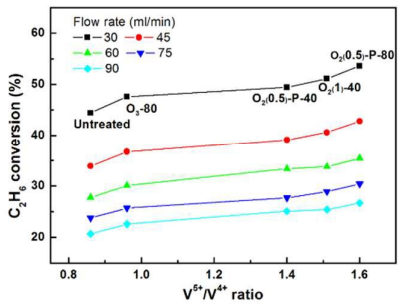

Fig. 7 Ethane conversion as a function of V^{5+}/V^{4+} molar ratio

4. Conclusions

As the first investigation, we proposed and successfully verified the novel method to improve the catalytic performance of MoVNbTe oxide catalyst by oxygen plasma. The basic idea is to increase the vanadium valence state (i.e., the active site for ODHE reaction) on the catalyst surface by using the oxidizing atmosphere of oxygen plasma or ozone.

The characterization results demonstrated that the oxygen plasma can effectively transform the surface vanadium from V^{4+} to V^{5+} without influencing the M1 phase structure. The oxidized catalysts showed improved catalytic performance in ODHE experiment, coinciding well with the pentavalent vanadium concentration. By using oxygen plasma to change the oxidation state of active sites in metal oxide catalyst, we provide a new means for catalyst modification. In addition, as a gas-solid phase treatment method, plasma treatment provides an efficient and mild way for catalyst preparation and modification. It is anticipated that this novel approach can be extended for a class of redox catalysts.

Acknowledgements

Financial supports from National Science and Technology Key Supporting Project (2013BAF08B05) and National Natural Science Foundation (No. 21176137) are acknowledged.

Notes and references

1. M. Zhang and Y. Yu, Ind. Eng. Chem. Res., 2013, **52**, 9505.
2. T. Ren, M. Patel and K. Blok, Energy, 2008, **33**, 817-833.
3. D. Sanfilippo and I. Miracca, Catal. Today, 2006, **111**, 133-139.
4. C. A. Carrero, R. Schloegl, I. E. Wachs and R. Schomaecker, ACS Catal., 2014, **4**, 3357-3380.
5. R. Koirala, R. Buechel, F. Krumeich, S. E. Pratsinis and A. Baiker, ACS Catal., 2015, **5**, 690-702.
6. F. Cavani, N. Ballarini and A. Cericola, Catal. Today, 2007, **127**, 113-131.
7. C. A. Gärtner, A. C. van Veen and J. A. Lercher, J. Am. Chem. Soc., 2014, **136**, 12691-12701.
8. P. Ciambelli, L. Lisi, R. Pirone, G. Ruoppolo and G. Russo, Catal. Today, 2000, **61**, 317-323.
9. S. Wang, K. Murata, T. Hayakawa, S. Hamakawa and K. Suzuki, Chem. Commun., 1999, 103-104.
10. T. Konya, T. Katou, T. Murayama, S. Ishikawa, M. Sadakane, D. Buttreyc and W. Ueda, Catal. Sci. Technol., 2013, **3**, 380-387.
11. P. Botella, A. Dejoz, J. Lopeznieto, P. Concepcion and M. Vazquez, Appl. Catal. A:Gen, 2006, **298**, 16-23.
12. J. M. L. P. Nieto, P. Botella, M. I. V Zquez and A. Dejoz, Chem. Commun., 2002, 1906-1907.
13. Q. Xie, L. Chen, W. Weng and H. Wan, J. Mol. Catal. A: Chem., 2005, **240**, 191-196.
14. B. Solsona, F. Ivars, A. Dejoz, P. Concepción, M. I. Vázquez and J. M. López Nieto, Top Catal., 2009, **52**, 751-757.
15. B. Solsona, T. Blasco, J. M. López Nieto, M. L. Peña, F. Rey and A. Vidal-Moya, J. Catal., 2001, **203**, 443-452.
16. E. Heracleous, M. Machli, A. A. Lemonidou and I. A. Vasalos, J. Mol. Catal. A: Chem., 2005, **232**, 29-39.
17. H. Zhu, P. Laveille, D. Rosenfeld, M. Hedhili and J. Basset , Catal. Sci. Technol., 2015, **5**, 4164-4173.
18. R. K. Grasselli, D. J. Buttrey, J. D. Burrington, A. Andersson, J. Holmberg, W. Ueda, J. Kubo, C. G. Lugmair and A. F. Volpe, Top Catal., 2006, **38**, 7-16.
19. B. Chu, L. Truter, T. A. Nijhuis and Y. Cheng, Catal. Sci. Technol., 2015, **5**, 2807-2813.
20. B. Chu, L. Truter, T. A. Nijhuis and Y. Cheng, Appl. Catal. A: Gen., 2015, **498**, 99-106.
21. B. Chu, H. An, T. A. Nijhuis, J. C. Schouten and Y. Cheng, J. Catal., 2015, **329**, 471-478.
22. R. G. R. Grasselli, J. B. J. Burrington, D. B. D. Buttrey, P. D. P. DeSanto, C. L. C. Lugmair, A. V. A. Volpe and T. W. T. Weingand, Top Catal., 2003, **23**, 5-22.
23. W. Ueda, D. Vitry and T. Katou, Catal. Today, 2004, **96**, 235-240.
24. P. DeSanto, D. Buttrey, R. Grasselli, C. Lugmair, A. Volpe, B. Toby and T. Vogt, Z. Kristallogr., 2004, **219**, 152-165.
25. R. K. Grasselli, D. J. Buttrey, P. DeSanto, J. D. Burrington, C. G. Lugmair, A. F. Volpe and T. Weingand, Catal. Today, 2004, **91-92**, 251-258.
26. M. Hävecker, S. Wrabetz, J. Kröhnert, L. Csepei, R. Naumann D Alnoncourt, Y. V. Kolen Ko, F. Girgsdies, R. Schlögl and A. Trunschke, J. Catal., 2012, **285**, 48-60.
27. T. T. Nguyen, B. Deniau, P. Delichere and J. M. Millet, Top Catal., 2014, **57**, 1152-1162.
28. X. YANG, R. FENG, W. JI and C. AU, J. Catal, 2008, 253, 57-65.
29. M. Œ. J. R. Boutonnet Kizling, Appl. Catal. A: Gen, 1996, **147**, 1-21.
30. N. Wang, K. Shen, X. Yu, W. Qian and W. Chu, Catal. Sci. Technol., 2013, **3**, 11885-11890.
31. C. Liu, G. P. Vissokov and B. W. L. Jang, Catal. Today, 2002, **72**, 173-184.
32. Z. Nazarpoor, S. Ma, P. T. Fanson, O. S. Alexeev and M. D. Amiridis, J. Catal., 2013, **3**, 2278-2287.
33. J. Liu, Z. Jiang, Z. Jiang and Y. Meng, J. Mater. Chem., 2011, **21**, 5565-5568.
34. G. Liu, Y. Li, W. Chu, X. Shi, X. Dai and Y. Yin, Catal. Commun., 2008, **9**, 1087-1091.
35. Z. Wang, Y. Zhao, L. Cui, H. Du, P. Yao and C. Liu, Green Chem., 2007, **9**, 554-559.
36. F. Holzer, F. D. Kopinke and U. Roland, Plasma Chem. Plasma P., 2005, **25**, 595-611.
37. Y. Guo, D. Ye, K. Chen, J. He and W. Chen, J. Mol. Catal. A: Chem., 2006, **245**, 93-100.
38. Y. Lin, Y. Hsu, S. Chen, L. Chen and K. Chen, J. Mater. Chem., 2010, **20**, 10611-10614.
39. J. Zou, Y. Zhang and C. Liu, Langmuir, 2006, **22**, 11388-11394.
40. B. Deniau, T. T. Nguyen, P. Delichere, O. Safonova and J. M. Millet, Top Catal, 2013, **56**, 1952-1962.
41. K. Kutasi, V. Guerra and P. A. Sá, Plasma Sources Sci. Technol., 2011, **20**, 035006.
42. Hsu-Hui Cheng, Shiao-Shing Chen and W. A. D. H. Yu-Chi, Environ. Eng. Manag. J., 2007, **17**, 427-433.
43. X. Zhu, P. Huo, Y. Zhang and C. Liu, Ind. Eng. Chem. Res., 2006, **45**, 8604-8609.
44. A. C. Sanfiz, T. W. Hansen, D. Teschner, P. Schnörch, F. Girgsdies, A. Trunschke, R. Schlögl, M. H. Looi and S. B. A. Hamid, J. Phys. Chem. C, 2010, **114**, 1912-1921.
45. G. Che-Galicia, R. Quintana-Solórzano, R. S. Ruiz-Martínez, J. S. Valente and C. O. Castillo-Araiza, Chem. Eng. J., 2014, **252**, 75-88.
46. R. Schlögl, Top Catal., 2011, **54**, 627-638.